

Article

Study on Corrosion Resistance of LDH/Micro-Arc Oxidation Composite Superhydrophobic Coatings on AZ31 Magnesium Alloy

Dongjie Liu ^{1,*} , Jing Liu ¹, Guangyu Liu ², Yuntao Xie ³ and Zongfan Duan ^{1,*} ¹ School of Materials Science and Engineering, Xi'an University of Technology, Xi'an 710048, China² School of Materials Science and Engineering, Northwestern Polytechnical University, Xi'an 710072, China³ School of Chemical Engineering, Sichuan University of Science and Engineering, Zigong 643000, China

* Correspondence: liudj2008@126.com (D.L.); duanzf@xaut.edu.cn (Z.D.); Tel.: +86-29-82312757 (D.L.); +86-29-82312172 (Z.D.)

Abstract: Because of some defects such as holes and cracks, the corrosion resistance of micro-arc oxidation coating needs to be improved by surface modification. In this paper, LDH/MAO film with a micro-/nano-structure is constructed on the surface of AZ31 magnesium alloy by controlling the composition and concentration of the hydrothermal solution. The superhydrophobic surface is successfully constructed by coating an OTES modifier on the surface of LDH/MAO film by the spin-coating method. The surface morphologies, contact angles, and corrosion resistance of composite coatings are tested. The results show that the OTES-LDH/MAO composite coatings of magnesium alloy can seal the defects in the MAO film well to achieve a superhydrophobic effect and better corrosion resistance. Compared with a MgO ceramic film, the water contact angle of OTES-LDH/MAO composite coatings is increased from 38° to 155°; the corrosion potential increases by 0.7 V, the corrosion current density and polarization resistance decreases and increases by four orders of magnitude, respectively; and the corrosion resistance becomes much higher than that of MAO film.

Keywords: magnesium alloy; micro-arc oxidation; layered double hydroxide; superhydrophobic; corrosion resistance



Citation: Liu, D.; Liu, J.; Liu, G.; Xie, Y.; Duan, Z. Study on Corrosion Resistance of LDH/Micro-Arc Oxidation Composite Superhydrophobic Coatings on AZ31 Magnesium Alloy. *Coatings* **2023**, *13*, 643. <https://doi.org/10.3390/coatings13030643>

Academic Editor: Michele Ferrari

Received: 15 February 2023

Revised: 6 March 2023

Accepted: 15 March 2023

Published: 18 March 2023



Copyright: © 2023 by the authors. Licensee MDPI, Basel, Switzerland. This article is an open access article distributed under the terms and conditions of the Creative Commons Attribution (CC BY) license (<https://creativecommons.org/licenses/by/4.0/>).

1. Introduction

Magnesium alloys have attracted widespread attention in many fields due to their high specific strength, low density, excellent castability, and stiffness [1–3]. Because they are highly reactive, magnesium alloys are more susceptible to corrosion than other alloys [3,4]. Therefore, surface-treatment techniques are used to form uniform, adherent, nonporous, or even self-healing films to effectively protect the Mg substrate from corrosion [5]. Various techniques, including micro-arc oxidation [6,7], chemical conversion films [8,9], superhydrophobic films [10,11], electro- or electroless metal plating [12,13], atmospheric plasma spraying [14], and sputtering deposition processes [15], have been widely applied to Mg alloys.

Micro-arc oxidation (MAO) is widely used in the surface treatment of magnesium, aluminum, and titanium. MAO coatings can improve the corrosion resistance of Mg alloys. Nevertheless, some micro-pores and micro-cracks appear in ceramic film, which reduce the corrosion resistance of the substrate at application [16]. Therefore, additional surface treatment techniques are required to effectively improve the corrosion properties of magnesium alloys [17–19]. Layered double hydroxide (LDH), with a brucite-like lamellar structure, consists of positively charged components containing the sheet and interlamellar area for the charge balance of anions and water molecules [20,21]. In recent years, LDH has been widely studied as an additive for films to improve the corrosion resistance of magnesium alloys [22,23]. Recently, more researchers have studied the preparation of LDH

on MAO film, which has enhanced the corrosion resistance of magnesium alloy by sealing the pores and cracks of the MAO film [24–26].

Superhydrophobicity, which has a water contact angle (WCA) above 150° on solid surfaces, has attracted great interest in the industry because of its special function. Typically, superhydrophobic surfaces are prepared by a two-step route in which micro-/nano-structures are created on the surface and then modified with low-surface-energy compounds [27]. Today, many of the manufacturing methods that have been reported for rough surfaces on magnesium alloys, for example, chemical etching, immersion, and wet chemical etching methods, are harmful to operators and can contaminate the environment [28]. Accordingly, we designed superhydrophobic surfaces by utilizing LDH microcrystals grown in the porous structure of MAO films with specific micro-/nano-structures.

In view of the fact that the MgO micro-arc oxidation ceramic film is porous and cannot meet the requirements for use, this study adopted a hydrothermal synthesis method to repair the holes, cracks, and other defects in MgO ceramic film by in situ growing an MgAl-LDH layer and constructed micro-/nano-structures on its surface. At the same time, the film was modified with octyltriethoxysilane (OTES) as a low-surface-energy substance to obtain an OTES-LDH/MAO composite coating, demonstrating the influence of hydrothermal synthesis concentration on the phase composition and surface morphology of the composite coating. The electrochemical performance of the films in NaCl solution and their wetting effect were studied.

2. Experimental

2.1. Materials and Pretreatment

Commercial AZ31 magnesium alloy sheet was selected as the experimental substrate; its composition included 2.5–3.0 wt% aluminum, 0.8–1.3 wt% zinc, 0.5–0.75 wt% manganese, and 0.13–0.15 wt% silicon, and the remaining was magnesium. All reagents were analytically pure and used as raw materials without further purification.

2.2. Processing Route

The method to prepare composite superhydrophobic coatings was as shown below. The AZ31 Mg substrate was successively polished with SiC sandpaper of different particle sizes (240–600–1000#) until the surface was bright, then washed with anhydrous ethanol in an ultrasonic cleaner for 5 min, and finally dried in a 60°C drying oven. The pretreatment of the sample was carried out by using type MAO75-III microcomputer-controlled automatic micro-arc oxidation equipment developed by the Xi'an University of Technology. AZ31 Mg alloys were immersed in Na_2SiO_3 solution including a small amount of NaOH and KF for 30 min with a constant voltage, and the experiments were carried out at 250 V, 300 V, and 350 V voltages. The positive pulse width was 50 μs , and the frequency was 600 Hz.

The sample after MAO was immersed in nitrate solution, and then LDH film was generated in situ with a hydrothermal reaction. The specific details were as follows: First, the mixed solution was prepared at room temperature with 0.05 M $\text{Mg}(\text{NO}_3)_2 \cdot 6\text{H}_2\text{O}$ and various concentrations of $\text{Al}(\text{NO}_3)_3 \cdot 9\text{H}_2\text{O}$ (0.01, 0.03, 0.05 M) and calibrated to $\text{pH} = 10$ with NaOH (2.0 M) solution. The solution was stirred on a magnetic stirrer to obtain a uniform hydrothermal solution and then filled into a Teflon-lined stainless-steel autoclave. Then, the MAO coating was placed in a hydrothermal solution and treated at 100°C for 18 h. The samples after hydrothermal reaction were washed and dried with deionized water, and MgAl-LDH/MAO composite film was prepared on the surface of the AZ31 Mg alloy samples.

The AZ31 magnesium alloy with an LDH/MAO composite film was placed on a KW-4A Spin Coater (Shanghai ZOLLO Industrial Co., Ltd., Shanghai, China). In the first stage, the spin coating time was 9 s, and the rotational speed was 600 r/min. In the second stage, the spin coating time was 20 s, and the rotational speed was 2100 r/min. In the first stage, the OTES solution was added to the surface of the sample. After the spin coating, the sample was placed into an electric blast drying oven to dry. After being

repeated several times, the OTES-LDH/MAO composite coatings were obtained. Figure 1 shows the schematic illustration for forming OTES-LDH/MAO composite coatings on AZ31 magnesium alloy.

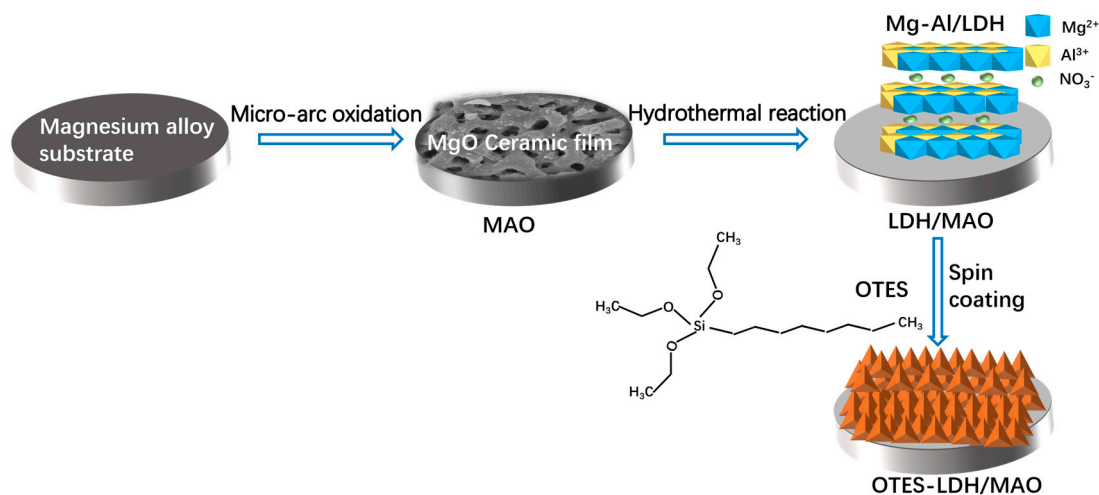


Figure 1. Schematic illustration for forming the OTES-LDH/MAO composite coatings.

2.3. Characterizations and Examinations

The surface morphologies of the composite coatings were observed with a scanning electron microscope (SEM). The phase composition of LDH/MAO films was studied using X-ray diffraction (XRD, 7000S) at a glancing angle of 1.5° using a Cu target (40 kV, 150 mA) within the range of $2\theta = 10\text{--}80^\circ$ and at a scanning rate of 4° min^{-1} . Under static conditions, the surface wettability of the sample was characterized by water-contact-angle measurements (WCA; JC2000A). The volume of the individual water droplet was fixed at $2 \mu\text{L}$. An electrochemical workstation (PARSTAT, 4000, USA) and a typical three-electrode cell were used for electrochemical measurements. A saturated calomel electrode (SCE) was used as the reference electrode, uncoated and coated AZ31 Mg alloy samples (exposed area, 1 cm^2) as the working electrode, and a platinum electrode as the counter electrode. Before measuring, the working electrode was immersed in corrosion media (3.5 wt% NaCl) until the cell open circuit potential (OCP) became stable. The polarization curve was subsequently measured from -0.5 to $+0.5$ V of the OCP with a scanning rate of 2 mV/s . The electrochemical impedance spectroscopy (EIS) measurements were performed from 10^{-1} Hz to 10^5 Hz with 10 points per decade and swept by a 10 mV RMS sinusoidal perturbation.

3. Results and Discussion

3.1. Phase Composition of LDH/MAO Film

Figure 2 illustrates the XRD patterns of the prepared MgAl-LDH/MAO film at different micro-arc oxidation voltages. It can be seen from Figure 2 that the samples had diffraction peaks of MgO (JPCDS: 45–0946) at $2\theta = 43.04^\circ$, 62.58° , 74.87° , and 78.86° , indicating that the AZ31 magnesium alloy formed a MgO ceramic layer after MAO treatment in the electrolyte of a sodium silicate system [29]. After the hydrothermal reaction, the sample had diffraction peaks of LDH (JPCDS: 89–0460) at $2\theta = 11.54^\circ$, 23.36° , and 39.20° , corresponding to the (003), (006), and (015) crystal planes, respectively. It also indicated the successful formation of the LDH on the MAO ceramic layer. Different crystal planes of LDH showed that the in situ generated MgAl-LDH exhibited better crystallinity and stronger diffraction peaks.

It can also be seen from Figure 2 that the diffraction peak intensity of MgO increased with the increase in voltage in the MAO process, which indicated that the content of MgO generated after MAO was higher with the increase in voltage. In addi-

tion, 350 V was selected for combination with the overall morphology of MAO film in subsequent experiments.

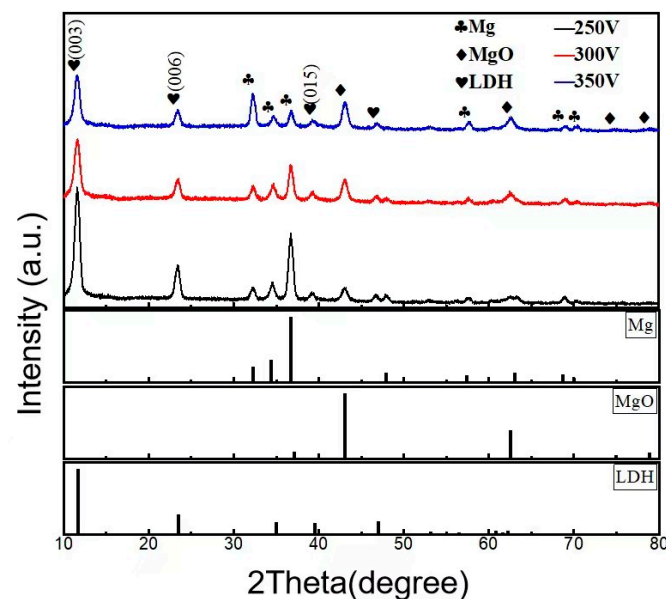


Figure 2. XRD patterns of LDH/MAO film.

3.2. Surface Morphologies of the As-Prepared Samples

As shown in Figure 3a, the surface of magnesium alloy after grinding, polishing, cleaning, and other pretreatment was still rough and uneven, and there were obvious scratches. As shown in Figure 3b, the surface of the MAO ceramic layer was distributed with micropores and microcracks with a diameter of about 0.1–1.8 μm , which is like the microscopic morphology formed by volcanic eruption and accumulation. Among them, the micropores are caused by the continuous breakdown discharge of the weak area on the surface of the ceramic layer, which leads to the increase in the size of the micropores. The microcracks are caused by the rapid cooling of the molten oxide in the high-temperature zone of the micro-arc discharge and the electrolyte, resulting in a large thermal stress, which leads to the appearance of microcracks. As shown in Figure 3c, compared with the MAO sample, the LDH/MAO film surface was composed of a large number of flakes growing perpendicular to the ceramic layer and was basically covered with holes and microcracks of the MAO ceramic layer. It also included some bulging shapes, which were caused by the thin sheet growth of the bulge part of the micro-arc oxidation ceramic layer. Based on SEM results, it could be inferred that part of the MgO in the micro-arc-oxidized ceramic coating that was dissolved to release Mg^{2+} combine with OH^- in alkaline hydrothermal solution to form $\text{Mg}(\text{OH})_2$ nano-sheets, which precipitated on the surface and in the pores of the ceramic layer. The Al^{3+} ions in the solution replaced some Mg^{2+} ions during the hydrothermal reaction, which precipitated in $\text{Mg}(\text{OH})_2$ in the MgO surface and holes to further form LDH nanometer tablets [30]. Figure 3d shows the micromorphology of OTES-LDH/MAO composite coatings. Compared with the LDH/MAO film shown in Figure 3c, the surface structure was denser and had fewer pores, and most nano-sheets were tiled on the surface after surface modification with OTES. Because of the composite effect of the micro-scale structure on the surface of the micro-arc oxidation ceramic layer and the nano-scale structure composed of the flakes in the hydrotalcite film, the obtained micro-/nano-structures provided a favorable basis for constructing super hydrophobic surfaces. After being modified with OTES, a low-surface-energy material, a superhydrophobic surface was constructed under the synergistic effect of three factors.

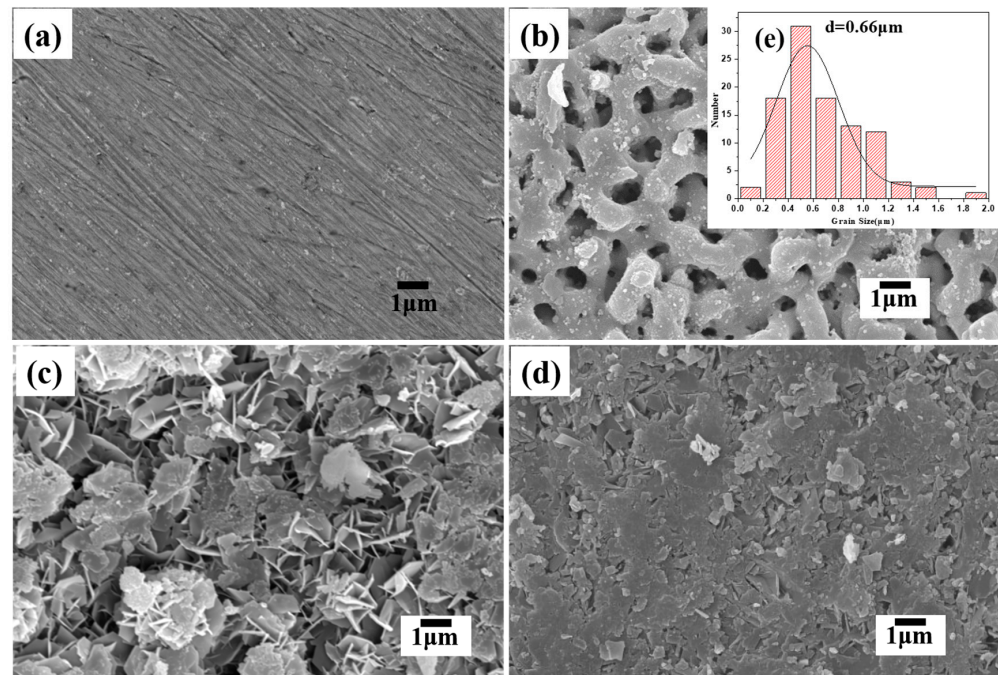


Figure 3. SEM images of Mg (a), MAO (b), LDH/MAO (c), and OTES-LDH/MAO (d); pore size of MAO (e).

3.3. Surface Wettability

Figure 4 shows the contact angle of the films prepared with different treatment methods. As shown in Figure 4a, Mg alloy is a type of hydrophilic material with an intrinsic oxidized layer. The surface contact angle of the Mg alloy was 53° .

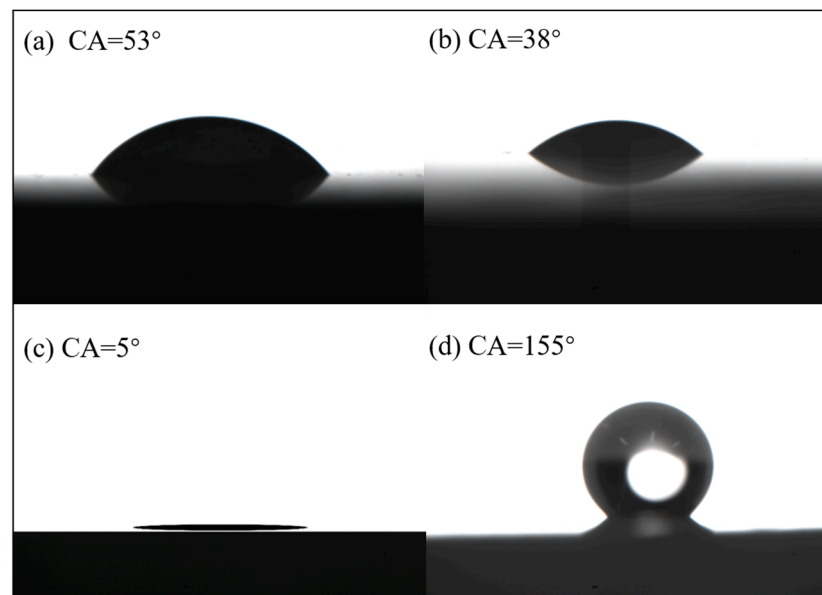


Figure 4. Static contact angles of various samples: (a) Mg substrate, (b) MAO, (c) LDH/MAO, and (d) OTES-LDH/MAO.

Figure 4b shows the contact angle image of the MAO film. The contact angle of the MAO film surface was 38° , which showed hydrophilicity. Water droplets easily diffuse on the surface and penetrate into the coating surface. This is mainly due to the hydrophilicity of the formed MgO film and the capillary force of the surface microporous structure. The

quantitative relationship between roughness and wettability on the MAO surface can be explained by the Wenzel equation, as shown in Equation (1).

$$\cos \theta^* = r \cos \theta \quad (1)$$

where θ^* is the contact angle of liquid on rough surface, also known as apparent contact angle; r is the roughness factor of the solid surface. According to the Wenzel model, roughness affects the hydrophilicity and hydrophobicity of solid surface. With the increase in roughness, the hydrophilic film is more hydrophilic, and the hydrophobic film is more hydrophobic, but the Wenzel model is only applicable to homogeneous surfaces [31]. Due to MgO presenting hydrophilic characteristics, the hydrophilicity of MAO film is increased, making the surface rougher via MAO technology.

Figure 4c shows the contact angle image of the LDH/MAO composite film. As shown in Figure 4c, the LDH/MAO composite film showed superhydrophilicity, and its contact angle was close to 5° . According to the analysis of surface morphology, the surface of LDH/MAO composite film was a micron-level layered structure. Moreover, through hydrothermal reaction, a large number of hydrophilic groups, such as OH^- , formed on the surface of the LDH/MAO composite film, which increased the surface energy and made the surface more hydrophilic [32].

Dropping OTES onto LDH/MAO film and then spin coating, its contact angle reached 155° , as shown in Figure 4d, realizing the transition from superhydrophilicity to superhydrophobicity. It is shown that surface roughness and surface chemical composition are essential factors in constructing superhydrophobic surfaces.

The reason for this superhydrophobic effect is that the micro/nano binary structure of the OTES-LDH/MAO composite coatings makes water droplets not completely in contact with the solid surface when they drop on this surface: only a small part contact with the solid surface. The rest is mostly in contact with the air trapped by the structure. This wetting state can be depicted by the Cassie–Baxter model, shown in Equation (2), which describes the relationship between apparent contact angle and rough structure by assuming that the rough surface is composed of solid phase and air. On the surface of preparing OTES-LDH/MAO, many concave pores are evenly distributed, which can easily trap air. As a water droplet is placed on the surface of OTES-LDH/MAO composite coatings, a composite contact is formed between the water droplet and the surface. Because water droplets can come into contact with solid surfaces and layers of air trapped in dimples,

$$\cos \theta_c = f_1 (\cos \theta_1 + 1) - 1 \quad (2)$$

where θ_c and θ_1 are the contact angles on rough and smooth surfaces, respectively; and f_1 is the fraction of solid–liquid contact area to total area. Because of that, the surface of LDH/MAO film has a contact angle of 5° , and the numeric value of f_1 was 0.047. This means that the LDH/MAO film has a hydrophilic property. Normally, a water droplet is suspended on OTES-coated MAO highlands, and the air pockets are trapped in dimples. The trapped air layer can greatly reduce the adhesion of water droplets to the surface, which in turn imparts the superhydrophobicity to the surface of OTES-LDH/MAO composite coatings.

3.4. Corrosion Resistance

Figure 5 shows the potentiodynamic polarization curves of different samples in 3.5 wt.% NaCl aqueous solution. The related electrochemical parameters are summarized in Table 1. The corrosion current density (I_{corr}) and corrosion potential (E_{corr}) of the film after different treatments could be obtained, and the polarization resistance (R_p) could be calculated by the Stein–Geary equation [33]. The instantaneous corrosion rate (P_i) from polarization curves was determined from the corrosion current density (I_{corr}) using $P_i = 22.85 I_{\text{corr}}$ [10].

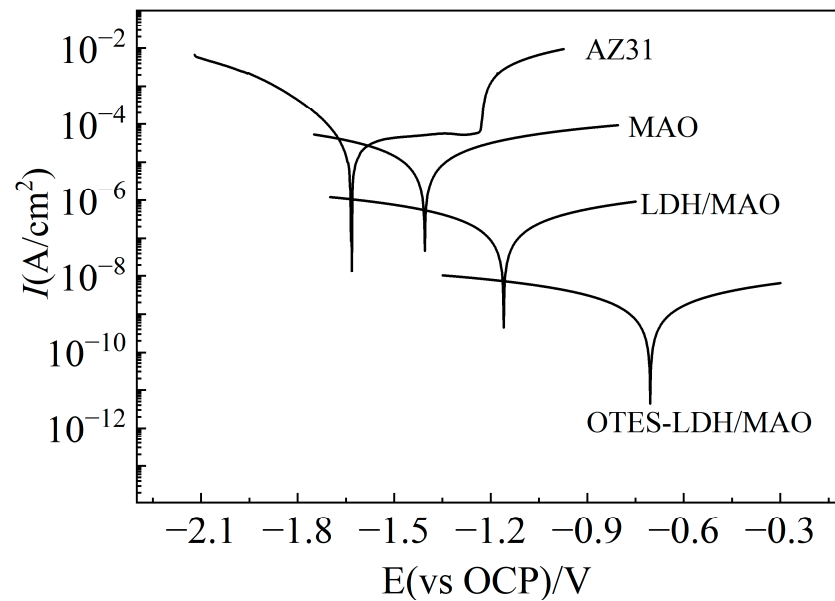


Figure 5. Polarization curves of various samples.

Table 1. Polarization parameters of various samples.

Samples	E_{corr}/V	$I_{\text{corr}}/\text{A}\cdot\text{cm}^{-2}$	$R_p/\Omega\cdot\text{cm}^2$	$P_i/\text{mm}\cdot\text{y}^{-1}$
AZ31	−1.5794	2.78×10^{-4}	93.91	6.35
MAO coating	−1.4049	4.02×10^{-6}	6479.9	0.09
LDH/MAO	−1.1595	5.70×10^{-8}	4.5764×10^5	1.30×10^{-3}
OTES-LDH/MAO	−0.7042	4.12×10^{-10}	6.3296×10^7	9.41×10^{-6}

Corrosion potential E_{corr} is a thermodynamic parameter that is mainly determined by the properties of the coating itself. The more positive the E_{corr} , the less the corrosion tendency. The corrosion current density I_{corr} is a kinetic parameter, and the lower the I_{corr} , the lower the corrosion rate [34]. According to the data in Table 1, the AZ31 magnesium alloy substrate had the maximum corrosion current density I_{corr} ($2.78 \times 10^{-4} \text{ A}\cdot\text{cm}^{-2}$), the most negative corrosion potential E_{corr} (−1.5794 V), and the minimum polarization resistance R_p ($93.91 \Omega\cdot\text{cm}^2$). The instantaneous corrosion rate of the AZ31B magnesium alloy in this case was about 6.35 mm/y. It can be seen that the corrosion resistance of the AZ31 magnesium alloy substrate is poor. The corrosion current density I_{corr} of the MAO layer decreased by two orders of magnitude to $4.02 \times 10^{-6} \text{ A}\cdot\text{cm}^{-2}$; the corrosion potential was −1.4049 V, which increased by 174.5 mV; and the polarization resistance (R_p) increased by nearly three orders of magnitude. The test results showed that the micro-arc oxidation treatment significantly improved the corrosion resistance of the magnesium alloy substrate. For the LDH/MAO film and OTES-LDH/MAO coatings, the corrosion current density further decreased to $5.70 \times 10^{-8} \text{ A}\cdot\text{cm}^{-2}$ and $4.12 \times 10^{-10} \text{ A}\cdot\text{cm}^{-2}$, respectively, compared with that of MAO film; and the hydrothermal synthesis LDH and low-surface-energy modification each decreased by two orders of magnitude at each step. The corrosion potential E_{corr} also showed a significant positive shift, and the corrosion potential of LDH was positively shifted 245.4 mV by hydrothermal synthesis on the basis of the MAO film. After continuous low-surface-energy modification with OTES, the corrosion potential shifted to 455.3 mV again. The corrosion current density I_{corr} decreased to $4.12 \times 10^{-10} \text{ A}\cdot\text{cm}^{-2}$, which is equivalent to a corrosion rate of about 0.009 $\mu\text{m}/\text{y}$. At the same time, the polarization resistance R_p increased by two orders of magnitude according to hydrothermal synthesis LDH and low-surface-energy modification. The results showed that the corrosion resistance of magnesium alloy can be significantly improved by obtaining LDH layer on

MAO layer, and the corrosion resistance of magnesium alloy can be further improved by low-surface-energy modification with OTES.

Figures 6 and 7 are Nyquist and Bode diagrams of the AZ31 substrate and three kinds of films, respectively. On the Nyquist diagram, the larger the radius of the capacitive arc, the smaller the corrosion rate and the better the corrosion resistance. The impedance diagram of the AZ31 substrate (Figure 7a) is composed of a high-frequency capacitive loop and a low-frequency inductive loop. The high-frequency capacitive loop corresponds to the corrosion product film, and the inductive loop indicates that the sample had anodic dissolution in the low-frequency band. From Figure 7b, it can be seen that the MAO film also displays two semicircle Nyquist plots, i.e., one capacitive loop at the high-frequency region and one capacitive loop at the low-frequency region. The LDH/MAO film and OTES-LDH/MAO-composited coatings display three semicircle Nyquist plots in the high-, medium-, and low-frequency regions (Figure 7c,d). It is clearly seen that the diameters of the capacitive loops of the corresponding OTES-LDH/MAO-composited coatings were significantly larger than those of the LDH/MAO film, MAO film, and AZ31 Mg alloy. According to the Nyquist impedance results, the corrosion resistance of the samples could be listed in an increasing order: AZ31 Mg alloy substrate < MAO < LDH/MAO < OTES-LDH/MAO, which was consistent with the polarization results (Figure 5).

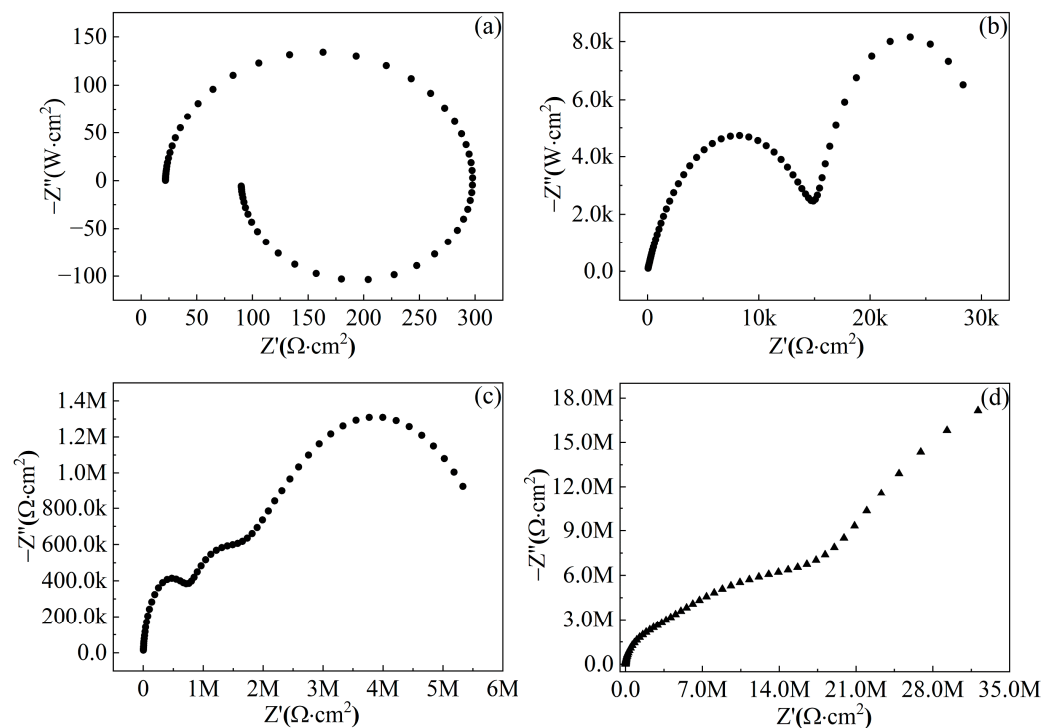


Figure 6. Nyquist plots of various samples by different treatment methods: (a) AZ31 substrate, (b) MAO, (c) LDH/MAO, and (d) OTES-LDH/MAO.

According to the Bode diagram, the greater the value of the impedance modulus $|Z|$ in the $f < 10$ Hz low-frequency area, the better the corrosion-resistant performance. It can be seen from Figure 8 that the arc radius of the AZ31 magnesium alloy substrate was very small, while the radius of the other three groups of samples after surface treatment was significantly increased by one order of magnitude. Corresponding to the Bode diagram, the surface-treated coating had obvious advantages in corrosion resistance compared with the substrate. It can be clearly seen from the Bode diagram shown in Figure 8 that the impedance modulus $|Z|$ of the three groups of samples grown with the coating after surface treatment was higher than that of the magnesium alloy matrix in all frequency ranges, especially the frequency range of less than 100 Hz. After micro-arc oxidation, hydrothermal

synthesis of LDH, and low-surface-energy modification treatment, the impedance modulus $|Z|_{f=0.1\text{Hz}}$ of the OTES-LDH/MAO composite coatings reached $5.4 \times 10^6 \Omega \cdot \text{cm}^2$. The impedance modulus of the MAO layer $|Z|_{f=0.1\text{Hz}}$ was $2.5 \times 10^4 \Omega \cdot \text{cm}^2$, the impedance modulus of the composite film layer was increased by two orders of magnitude, and the corrosion resistance of the AZ31 magnesium alloy substrate significantly improved.

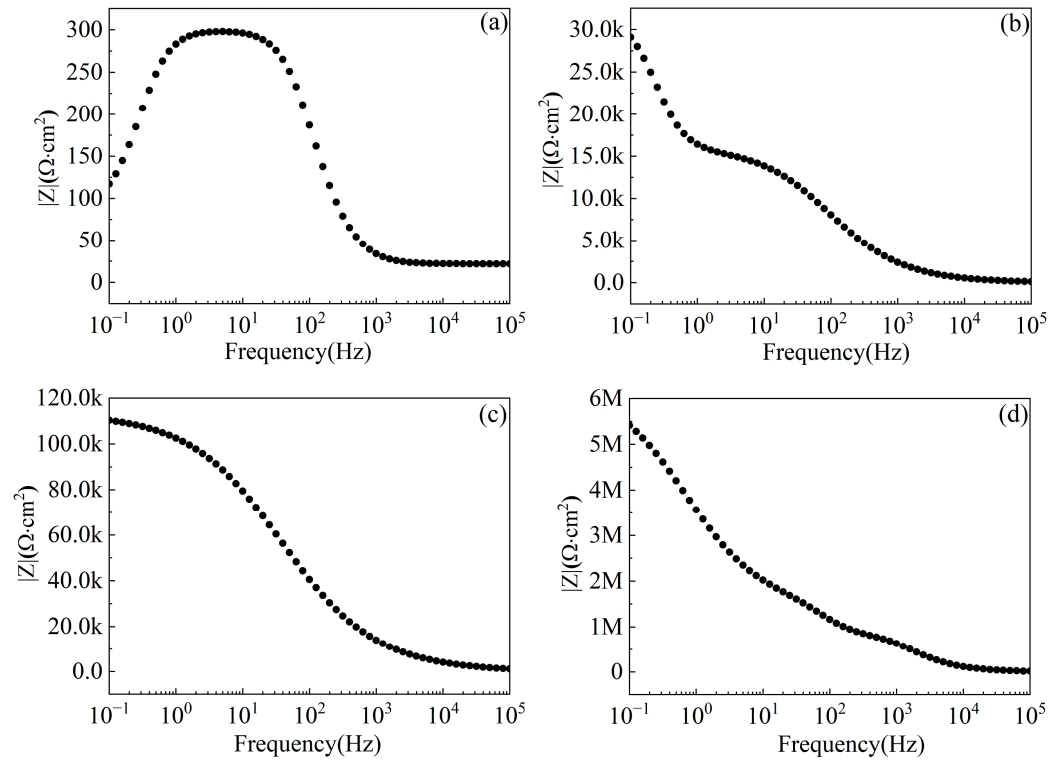


Figure 7. Bode plots of $|Z|$ vs. frequency of various samples by different treatment methods: (a) AZ31 substrate, (b) MAO, (c) LDH/MAO, and (d) OTES-LDH/MAO.

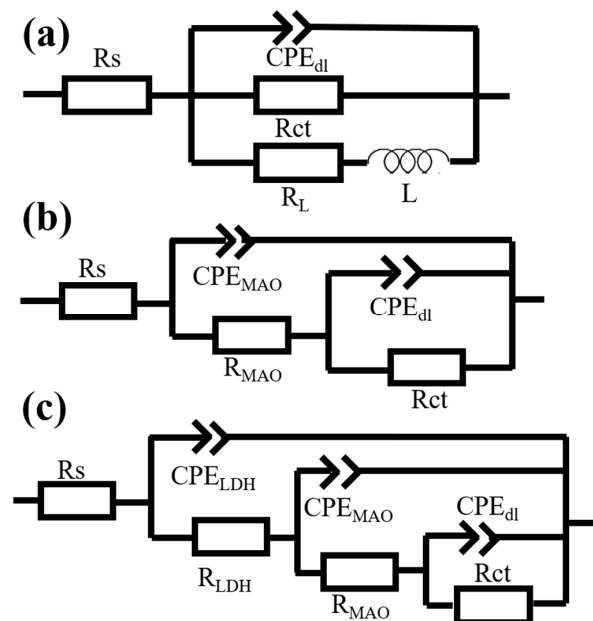


Figure 8. Equivalent circuits of various samples by different treatment methods: (a) AZ31 substrate, (b) MAO, (c) LDH/MAO, and (d) OTES-LDH/MAO.

Based on the above experimental results, electroequivalent circuits (ECs) were proposed and presented in Figure 8. Different equivalent circuits were used to fit the EIS for the uncoated sample and coated samples [35–37]. The fitted parameters of the EIS plots are shown in Table 2. In Figure 8, R_s and R_{ct} indicate the solution resistance and charge transfer resistance, respectively. Constant phase element (CPE), which is related to the capacitance of electrical double layer (CPE_{dl}), was used to replace the pure capacitor to increase fitting accuracy. According to Table 2, which shows the parameters obtained after immersion of the samples in 3.5 wt.% NaCl aqueous solution, compared with MAO-, LDH/MAO-, and OTES-LDH/MAO-coated samples, the lower R_{ct} of $68 \Omega \cdot \text{cm}^2$ of the AZ31 Mg alloy indicated poor corrosion performance. It was clearly seen that the OTES-LDH/MAO composite coating exhibited the best corrosion performance as well. For instance, the R_{MAO} for MAO and LDH/MAO films was 16.14 and $799.6 \text{ K}\Omega \cdot \text{cm}^2$, respectively, whereas that for OTES-LDH/MAO coatings increased to $24.95 \text{ M}\Omega \cdot \text{cm}^2$. These indicated that the LDH nano-sheets were formed on the surface and in the pores of the ceramic layer. It made the ceramic layer denser, resulting in higher R_{MAO} . At the same time, the R_{ct} for MAO film, LDH/MAO film, and OTES-LDH/MAO coatings was 0.0157, 4.611, and $44.93 \text{ M}\Omega \cdot \text{cm}^2$, respectively. The values of R_{ct} sequentially increased, indicating that the corrosion resistance of the coatings gradually improved. In summary, the MgAl-LDH film has good corrosion resistance to magnesium alloy, which can be significantly enhanced after modification with OTES.

Table 2. The corresponding fitted parameters of the EIS plots for different samples.

Sample	Bare AZ31	MAO	LDH/MAO	OTES-LDH/MAO
$R_s/\Omega \cdot \text{cm}^2$	21.89	23.85	31.72	36.76
$CPE_{LDH}/\Omega^{-1} \cdot \text{cm}^{-2} \cdot \text{s}^{-n}$	—	—	2.875×10^{-10}	1.767×10^{-10}
n_{LDH}	—	—	0.9286	0.9517
$R_{LDH}/\Omega \cdot \text{cm}^2$	—	—	9.088×10^5	2.803×10^6
$CPE_{MAO}/\Omega^{-1} \cdot \text{cm}^{-2} \cdot \text{s}^{-n}$	—	1.052×10^{-6}	2.468×10^{-9}	1.019×10^{-8}
n_{MAO}	—	0.6743	1	0.5264
$R_{MAO}/\Omega \cdot \text{cm}^2$	—	1.614×10^4	7.996×10^5	2.495×10^7
$CPE_{dl}/\Omega^{-1} \cdot \text{cm}^{-2} \cdot \text{s}^{-n}$	8.069×10^{-6}	4.866×10^{-5}	1.02×10^{-7}	4.553×10^{-8}
n_{dl}	0.9793	1	0.6257	0.9015
$R_{ct}/\Omega \cdot \text{cm}^2$	68	1.57×10^4	4.611×10^6	4.493×10^7
$R_L/\Omega \cdot \text{cm}^2$	208.8	—	—	—
$L/H \cdot \text{cm}^{-2}$	91.07	—	—	—

According to the results of the Nyquist diagram and Bode diagram, it can be concluded that the ceramic film layer after micro-arc oxidation had certain corrosion resistance compared with that of the magnesium alloy. The LDH/MAO film layer can play a role in certain filling of the micropores on ceramic film layers. The LDH coating has an anion exchange effect, which can improve the corrosion resistance of film layers. The hydrotalline film with nanostructures can be better combined with other substances, and the corrosion resistance is further improved after the addition of modifiers with hydrophobic properties. It can be clearly seen that the corrosion resistance of the OTES-LDH/MAO composite coatings was the best.

4. Conclusions

A MgO ceramic layer was prepared via a micro-arc oxidation process. A MgAl-LDH film with anion exchange characteristics was obtained through the hydrothermal treatment of a magnesium MAO film. The LDH/MAO film has a micro-/nano-porous structure and superhydrophilicity. Compared with magnesium the MAO film, the LDH/MAO film exhibited higher compactness and significant enhancement in corrosion resistance in NaCl solution. After the low-surface-energy modification treatment of OTES by the spin-coating method, the wettability of the OTES-LDH/MAO composite coatings changed from

superhydrophilic of LDH/MAO film to superhydrophobic, and the water contact angle reached 155° , realizing the superhydrophobic effect. The OTES-LDH/MAO composite coatings had the lowest corrosion current density ($4.12 \times 10^{-10} \text{ A}\cdot\text{cm}^{-2}$), the most positive corrosion potential (-0.70 V), and the largest impedance modulus ($5.4 \times 10^6 \Omega\cdot\text{cm}^2$), showing better corrosion resistance. All these results provide new insights into the superior corrosion protection of magnesium alloy.

Author Contributions: Methodology, D.L. and Z.D.; validation, G.L. and J.L.; data curation, Y.X. and D.L.; writing—original draft preparation, D.L.; writing—review and editing, D.L. and Z.D.; supervision and funding acquisition, J.L. All authors have read and agreed to the published version of the manuscript.

Funding: This work was supported by the project of the National Natural Science Foundation of China (61404107, 52001251), Opening Project of Material Corrosion and Protection Key Laboratory of Sichuan province (2021CL06), and Opening Project of Key Laboratories of Fine Chemicals and Surfactants in Sichuan Provincial Universities (2018JXY08, 2021JXY04).

Institutional Review Board Statement: Not applicable.

Informed Consent Statement: Not applicable.

Data Availability Statement: Not applicable.

Conflicts of Interest: The authors declare no conflict of interest.

References

1. Predoi, D.; Ciobanu, S.C.; Iconaru, S.L.; Predoi, M.V. Influence of the Biological Medium on the Properties of Magnesium Doped Hydroxyapatite Composite Coatings. *Coatings* **2023**, *13*, 409. [\[CrossRef\]](#)
2. Xin, T.Z.; Zhao, Y.H.; Mahjoub, R.; Jiang, J.X.; Yadav, A.; Nomoto, K.; Niu, R.M. Ultrahigh Specific Strength in a Magnesium Alloy Strengthened by Spinodal Decomposition. *Sci. Adv.* **2021**, *23*, 1–9. [\[CrossRef\]](#)
3. Emelyanenko, K.A.; Chulkova, E.V.; Semiletov, A.M.; Domantovsky, A.G.; Palacheva, V.V.; Emelyanenko, A.M.; Boinovich, L.B. The Potential of the Superhydrophobic State to Protect Magnesium Alloy against Corrosion. *Coatings* **2022**, *12*, 74. [\[CrossRef\]](#)
4. Cao, F.Y.; Shi, Z.M.; Song, G.L.; Liu, M.; Dargusch, M.S.; Atrensa, A. Stress Corrosion Cracking of Several Solution Heat-Treated Mg–X Alloys. *Corros. Sci.* **2015**, *96*, 121–132. [\[CrossRef\]](#)
5. Wang, X.J.; Xu, D.K.; Wu, R.Z.; Chen, X.B.; Peng, Q.M.; Jin, L. What Is Going on in Magnesium Alloys. *J. Mater. Sci. Technol.* **2018**, *34*, 245–247. [\[CrossRef\]](#)
6. Vladimirov, B.V.; Krit, B.L.; Lyudin, V.B.; Morozova, N.V.; Rossiiskaya, A.D.; Suminov, I.V.; Epel'feld, A.V. Microarc Oxidation of Magnesium Alloys: A Review. *Surf. Eng. Appl. Electrochem.* **2014**, *50*, 195–232. [\[CrossRef\]](#)
7. Askarnia, R.; Fardi, S.R.; Sobhani, M.; Staji, H.; Aghamohammadi, H. Effect of Graphene Oxide on Properties of AZ91 Magnesium Alloys Coating Developed by Micro-Arc Oxidation Process. *J. Alloys Compd.* **2022**, *892*, 162106. [\[CrossRef\]](#)
8. Chen, X.B.; Yang, H.Y.; Abbott, T.B.; Easton, M.A.; Birbilis, N. Corrosion Protection of Magnesium and Its Alloys by Metal Phosphate Conversion Coatings. *Surf. Eng.* **2014**, *30*, 871–879. [\[CrossRef\]](#)
9. Dong, Q.S.; Ba, Z.X.; Jia, Y.Q.; Chen, Y.J.; Lv, X.Y.; Zhang, X.B.; Wang, Z.Z. Effect of Solution Concentration on Sealing Treatment of Mg–Al Hydrotalcite Film on AZ91D Mg Alloy. *J. Magnes. Alloys* **2017**, *5*, 320–325. [\[CrossRef\]](#)
10. Gu, C.D.; Yan, W.; Zhang, J.L.; Tu, J.P. Corrosion Resistance of AZ31B Magnesium Alloy with a Conversion Coating Produced from a Choline Chloride-Urea Based Deep Eutectic Solvent. *Corros. Sci.* **2016**, *106*, 108–116. [\[CrossRef\]](#)
11. Cui, L.Y.; Liu, H.P.; Zhang, W.L.; Han, Z.Z.; Deng, M.X.; Zeng, R.C. Corrosion Resistance of a Superhydrophobic Micro-Arc Oxidation Coating on Mg–4Li–1Ca Alloy. *J. Mater. Sci. Technol.* **2017**, *33*, 1263–1271. [\[CrossRef\]](#)
12. Zhang, W.X.; Jiang, Z.H.; Li, G.Y.; Jiang, Q.; Lian, J.S. Electroless Ni–Sn–P Coating on AZ91D Magnesium Alloy and Its Corrosion Resistance. *Surf. Coat. Technol.* **2008**, *202*, 2570–2576. [\[CrossRef\]](#)
13. Bakkar, A.; Neubert, V. Electrodeposition onto Magnesium in Air and Water Stable Ionic Liquids: From Corrosion to Successful Plating. *Electrochem. Commun.* **2008**, *9*, 2428–2435. [\[CrossRef\]](#)
14. Istrate, B.; Mareci, D.; Munteanu, C.; Stanciu, S.; Luca, D.; Crimu, C.I.; Kamel, E. In vitro electrochemical properties of biodegradable ZrO₂–CaO coated MgCa alloy using atmospheric plasma spraying. *J. Optoelectron. Adv. Mater.* **2015**, *17*, 1186–1192.
15. Song, G.L.; Unocic, K.A.; Meyer, H., III; Cakmak, E.; Brady, M.P.; Gannon, P.E.; Himmer, P.; Andrews, Q. The Corrosion and Passivity of Sputtered Mg–Ti Alloys. *Corros. Sci.* **2016**, *104*, 36–46. [\[CrossRef\]](#)
16. Simchen, F.; Sieber, M.; Kopp, A.; Lampke, T. Introduction to Plasma Electrolytic Oxidation—An Overview of the Process and Applications. *Coatings* **2020**, *10*, 628. [\[CrossRef\]](#)
17. Song, X.H.; Lu, J.H.; Yin, X.J.; Jiang, J.P.; Wang, J. The effect of pulse frequency on the electrochemical properties of micro arc oxidation coatings formed on magnesium alloy. *J. Magnes. Alloys* **2012**, *1*, 318–322. [\[CrossRef\]](#)

18. Zheng, Z.R.; Zhao, M.C.; Tan, L.L.; Zhao, Y.C.; Xie, B.; Yin, D.F.; Yang, K.; Atrens, A. Corrosion Behavior of a Self-Sealing Coating Containing CeO₂ Particles on Pure Mg Produced by Micro-Arc Oxidation. *Surf. Coat. Technol.* **2020**, *386*, 125456. [[CrossRef](#)]
19. Atapour, M.; Blawert, C.; Zheludkevich, M.L. The Wear Characteristics of CeO₂ Containing Nanocomposite Coating Made by Aluminate-Based PEO on AM 50 Magnesium Alloy. *Surf. Coat. Technol.* **2019**, *357*, 626–637. [[CrossRef](#)]
20. Razzaq, A.; Ali, S.; Asif, M.; In, S. Layered Double Hydroxide (LDH) Based Photocatalysts: An Outstanding Strategy for Efficient Photocatalytic CO₂ Conversion. *Catalysts* **2020**, *10*, 1185. [[CrossRef](#)]
21. Boumeriame, H.; Da Silva, E.S.; Cherevan, A.S.; Chafik, T.; Faria, J.L.; Eder, D. Layered Double Hydroxide (LDH)-Based Materials: A Mini-Review on Strategies to Improve the Performance for Photocatalytic Water Splitting. *J. Energy Chem.* **2022**, *64*, 406–431. [[CrossRef](#)]
22. Ishizaki, T.; Chiba, S.; Watanabe, K.; Hikaru, S. Corrosion Resistance of Mg-Al Layered Double Hydroxide Container-Containing Magnesium Hydroxide Films Formed Directly on Magnesium Alloy by Chemical-Free Steam Coating. *J. Mater. Chem. A* **2013**, *1*, 8968–8977. [[CrossRef](#)]
23. Ishizaki, T.; Kamiyama, N.; Watanabe, K.; Serizawa, A. Corrosion Resistance of Mg(OH)₂/Mg-Al Layered Double Hydroxide Composite Film Formed Directly on Combustion-Resistant Magnesium Alloy AMCa602 by Steam Coating. *Corros. Sci.* **2015**, *92*, 76–84. [[CrossRef](#)]
24. Kamiyama, N.; Panomsuwan, G.; Yamamoto, E.; Sudare, T.; Saito, N.; Ishizaki, T. Effect of Treatment Time in the Mg(OH)₂/Mg-Al LDH Composite Film Formed on Mg Alloy AZ31 by Steam Coating on the Corrosion Resistance. *Surf. Coat. Technol.* **2015**, *286*, 172–177. [[CrossRef](#)]
25. Dou, B.J.; Wang, Y.Q.; Zhang, T.; Liu, B.; Shao, Y.W.; Meng, G.Z.; Wang, F.H. Growth Behaviors of Layered Double Hydroxide on Microarc Oxidation Film and Anti-Corrosion Performances of the Composite Film. *J. Electrochem. Soc.* **2016**, *163*, C917. [[CrossRef](#)]
26. Kuznetsov, B.; Serdechnova, M.; Tedim, J.; Starykevich, M.; Kallip, S.; Oliveira, M.P.; Hack, T.; Nixon, S.; Ferreira, M.G.S.; Zheludkevich, M.L. Sealing of Tartaric Sulfuric (TSA) Anodized AA2024 with Nanostructured LDH Layers. *RSC Adv.* **2016**, *6*, 13942–13952. [[CrossRef](#)]
27. Yeganeh, M.; Mohammadi, N. Superhydrophobic Surface of Mg Alloys: A Review. *J. Magnes. Alloys* **2018**, *6*, 59–70. [[CrossRef](#)]
28. Zhou, M.; Pang, X.; Wei, L.; Gao, K. In situ Grown Superhydrophobic Zn-Al Layered Double Hydroxides Films on Magnesium Alloy to Improve Corrosion Properties. *Appl. Surf. Sci.* **2015**, *337*, 172–177. [[CrossRef](#)]
29. Wang, Z.H.; Zhang, J.M.; Bai, L.J.; Zhang, G.J. Effects of Al³⁺ concentration in hydrothermal solution on the microstructural and corrosion resistance properties of fabricated MgO ceramic layer on AZ31 magnesium alloy. *Mater. Corros.* **2020**, *72*, 620–632. [[CrossRef](#)]
30. Wang, Z.H.; Zhang, J.M.; Bai, L.J.; Zhang, G.J. Effect of Hydrothermal Treatment on Microstructure and Corrosion Resistance of Micro Arc Oxidation Ceramic Layer on AZ31 Mg-alloy. *Chin. J. Mater. Res.* **2020**, *34*, 183–190.
31. Wang, Z.W.; Wu, T.Z. Modeling pressure stability and contact angle hysteresis of superlyophobic surfaces based on local contact line. *J. Phys. Chem. C* **2015**, *119*, 12916–12922. [[CrossRef](#)]
32. Wu, L.; Wu, J.H.; Zhang, Z.Y.; Zhang, C.; Zhang, Y.X. Corrosion resistance of fatty acid and fluoroalkylsilane-modified hydrophobic Mg-Al LDH films on anodized magnesium alloy. *Appl. Surf. Sci.* **2019**, *487*, 569–580. [[CrossRef](#)]
33. Duan, H.P.; Yan, C.W.; Wang, F.H. Effect of Electrolyte Additives on Performance of Plasma Electrolytic Oxidation Films Formed on Magnesium Alloy AZ91D. *Electrochim. Acta* **2007**, *52*, 3785–3793. [[CrossRef](#)]
34. Ma, R.Z.; Jiang, M.H.; Xu, Z. *Introduction to Functional Materials Science*; Metallurgical Industry Press: Beijing, China, 2006.
35. Yao, Z.P.; Xia, Q.X.; Chang, L.M.; Li, C.N.; Jiang, Z.H. Structure and Properties of Compound Coatings on Mg Alloys by Micro-Arc Oxidation/Hydrothermal Treatment. *J. Alloys Compd.* **2015**, *633*, 435–442. [[CrossRef](#)]
36. Luo, D.; Liu, Y.; Yin, X.M.; Wang, H.Y.; Han, Z.W.; Ren, L.Q. Corrosion Inhibition of Hydrophobic Coatings Fabricated by Micro-Arc Oxidation on an Extruded Mg-5Sn-1Zn Alloy Substrate. *J. Alloys Compd.* **2018**, *731*, 731–738. [[CrossRef](#)]
37. Zhang, G.; Tang, A.T.; Wu, L.; Zhang, Z.Y.; Liao, H.X.; Long, Y.; Li, L.J.; Atrens, A.; Pan, F.S. In-Situ Grown Super- or Hydrophobic Mg-Al Layered Double Hydroxides Films on the Anodized Magnesium Alloy to Improve Corrosion Properties. *Surf. Coat. Technol.* **2019**, *366*, 238–247. [[CrossRef](#)]

Disclaimer/Publisher's Note: The statements, opinions and data contained in all publications are solely those of the individual author(s) and contributor(s) and not of MDPI and/or the editor(s). MDPI and/or the editor(s) disclaim responsibility for any injury to people or property resulting from any ideas, methods, instructions or products referred to in the content.